Cross Talk between Activation and Slow Inactivation Gates of *Shaker* Potassium Channels

Gyorgy Panyi[1] and Carol Deutsch[2]

[1]Department of Biophysics and Cell Biology, University of Debrecen, 4032 Debrecen, Hungary
[2]Department of Physiology, University of Pennsylvania, Philadelphia, PA 19104

This study addresses the energetic coupling between the activation and slow inactivation gates of *Shaker* potassium channels. To track the status of the activation gate in inactivated channels that are nonconducting, we used two functional assays: the accessibility of a cysteine residue engineered into the protein lining the pore cavity (V474C) and the liberation by depolarization of a Cs^+ ion trapped behind the closed activation gate. We determined that the rate of activation gate movement depends on the state of the inactivation gate. A closed inactivation gate favors faster opening and slower closing of the activation gate. We also show that hyperpolarization closes the activation gate long before a channel recovers from inactivation. Because activation and slow inactivation are ubiquitous gating processes in potassium channels, the cross talk between them is likely to be a fundamental factor in controlling ion flux across membranes.

INTRODUCTION

The principal mission of ion channels is to regulate the flow of ions across membranes. To this end channels exploit the two structural features, pores and gates, that distinguish them from other membrane proteins. The coordinated function of these pores and gates underlies electrical events in organisms as diverse as bacteria and man. Normal gated access to the pore requires a choreographed opening and closing of gates in response to a variety of stimuli. Consequently, abnormalities of gating may lead to pathophysiology (e.g., long QT syndrome in cardiac tissue, abnormal action potential firing, or transmitter release in neuronal tissue; Ashcroft, 2000). Furthermore, the allosteric coupling among different gates of the same ion channel provides a means for enhancing the subtleties and range of ion channel function.

Voltage-gated potassium (Kv) channels in the *Shaker* subfamily have three well-studied gates: an activation gate and two types of inactivation gates. These two inactivation gates, which typically prevent ion flow through depolarized channels, correspond to processes originally designated N-type and C-type inactivation. In general, N-type inactivation is the faster of the two, leading to the name "slow inactivation" for the latter. The activation gate is formed by a four-helix bundle at the cytoplasmic end of the pore, specifically by the C-terminal region of the sixth transmembrane segment (S6) of each of the four subunits of Kv channels (Liu et al., 1997; del Camino et al., 2000; del Camino and Yellen, 2001). The fast inactivation gate, lacking in many Kv channels, is composed of the cytosolic N terminus,

which snakes up into the cavity of the channel and blocks conductance (Hoshi et al., 1990; Choi et al., 1991; Demo and Yellen, 1991; Zhou et al., 2001a). Virtually all Kv channels possess a slow inactivation gate that closes by a cooperative rearrangement of regions in the outer mouth of the pore and selectivity filter in response to prolonged depolarization (Hoshi et al., 1991; Ogielska et al., 1995; Panyi et al., 1995; Liu et al., 1996; Loots and Isacoff, 1998).

In the simplest depiction, these gates can each assume either of two positions, open or closed. Thus, there are four composite gating states to consider, as shown in Fig. 1 A. For convenience, we refer to the slow inactivation gate simply as the inactivation gate. By this we mean a region in (or near) the selectivity filter that operationally functions as a gate. We assign names to the four composite gating states according to standard terminology, where C and O represent the closed and open conformations of the activation gate, respectively, and I indicates that the inactivation gate is closed (Fig. 1, A and B). The only completely open (i.e., conducting) state in this depiction is state O, because closure of either gate prevents ion flux. Note that this representation focuses on the gates and ignores the many conformational states that are known to be associated with each of these composite states, especially the many conformations the channel can assume when the activation gate is closed. In the diagram in Fig. 1 B, left-to-right movement (C→O or CI→OI) is opening of the activation gate in response to a depolarization, and movement

---

Correspondence to Carol Deutsch: cjd@mail.med.upenn.edu

from top to bottom (C→CI or O→OI) is closing of the inactivation gate.

Although the movements of these individual gates have been studied extensively in isolation (Yellen, 1998), the way in which these gates are energetically and kinetically coupled is less well understood. It is known that N- and C-type inactivation coexist and that N-type can speed C-type inactivation (Baukrowitz and Yellen, 1995), but the relationship between the activation gate and the slow inactivation gate has not been elucidated. What is the order and timing of movement of these two gates after a change of membrane potential? Does the state of one gate affect the movement of the other? If these two gates operate independently, then the time- and voltage-dependent state of the activation gate will be oblivious to whether the inactivation gate is open or closed.

To test this hypothesis, we investigated the status of the activation gate during entry into and recovery from slow inactivation. Our findings indicate that the rate of activation gate movement depends on the state of the inactivation gate. Closure of the inactivation gate slows closing of the activation gate at negative voltages and speeds its opening. Moreover, we show that hyperpolarization closes the activation gate long before a channel recovers from inactivation.

MATERIALS AND METHODS

Cell Culture
Human embryonic kidney cells transformed with SV40 large T antigen (*tsA201*) were grown in Dulbecco's minimum essential medium–high glucose supplemented with 10% FBS, 2 mM L-glutamine, 100 U/ml penicillin-G, and 100 μg/ml streptomycin (Invitrogen) at 37°C in a 9% CO_2 and 95% air-humidified atmosphere. Cells were passaged twice per week after a 7-min incubation in Versene containing 0.2 g EDTA/L (Invitrogen).

DNA Clones and Site-directed Mutagenesis
Modified *Shaker*-IR in a GW1-CMV mammalian expression plasmid, under the control of a highly expressing Kozak consensus promoter sequence (Kozak, 1991), was provided by R. Horn (Thomas Jefferson University, Philadelphia, PA) (Ding and Horn, 2002). This construct includes a deletion of amino acids 6–46 to remove N-type inactivation and C301S and C308S point mutations (Holmgren et al., 1996). These two mutations are necessary to exclude possible methanethiosulfonate ethyltrimethylammonium (MTSET; Toronto Research Corp.) modification of endogenous *Shaker* cysteines and accompanying functional effects. Amino acid substitutions at position 449 (T449A) and 474 (V474C) were introduced using a site-directed mutagenesis kit (QuikChange; Stratagene). Mutants were sequenced at the University of Pennsylvania School of Medicine DNA Sequencing Facility using a 16-capillary sequencing apparatus (ABI 3100; Applied Biosystems, Inc.) with BigDye Taq FS Terminator (version 3.1; Applied Biosystems, Inc.) chemistry. A Calcium Phosphate Transfection Kit (Invitrogen) was used to cotransfect CD8 carried in a EBO-pcD vector (Margolskee et al., 1988, 1993) with the *Shaker-IR* T449A/V474C construct using 4 or 10 μg of CD8 or *Shaker*-IR DNA, respectively, per 100-mm dish of *tsA201* cells. Transfected cells were replated onto 35-mm polystyrene cell cul-

ture dishes (Corning) pretreated with poly–L-ornithine (Sigma-Aldrich) to improve cell adhesion for excising patches. 12–36 h after transfection, current was recorded from transfected cells, which were identified by decoration with anti-CD8 antibody-coated Dynabeads (Dynal) as described previously (Margolskee et al., 1993; Jurman et al., 1994).

Electrophysiology
Standard methods were used to record currents in inside-out patches. Data were acquired using a HEKA EPC-9 amplifier, digitized with an ITC-16 analogue-to-digital converter (HEKA Elektronik, GmbH). The filter frequency was set to less than or equal to half the sampling frequency. Pipettes pulled from lead-free 8520 glass (Warner Instruments) were 8–9 MΩ and coated with R-6101 elastomer (Essex Group, Inc.) and fire polished. Adjustments for bath-pipette liquid junction potentials were made before current recording. Typical current amplitudes were 300–600 pA at +50 mV test potential, allowing the recording of macroscopic currents. Only those cells with a steady-state current <5% of the peak current were used in these experiments. Inside-out currents are plotted with reversed polarity for easier comparison with conventional whole-cell currents. In general, all holding potentials were −120, and voltage errors were <3 mV after series resistance compensation. All experiments were performed at room temperature (20–24°C). Data were analyzed using Pulse + PulseFit software (version 8.77; HEKA Elektronik, Dr. Schulze, GmbH). Reported errors are SEM.

Solutions
The standard intracellular (bath) solution contained 105 mM KF, 35 mM KCl, 10 mM EGTA, and 10 mM HEPES titrated to pH 7.36–7.38 with KOH for a final concentration of 160–165 mM K^+ and an osmolarity of 285–295 mOsm. For Cs liberation experiments, the standard intracellular solution was identical except that it contained 105 CsF and 35 CsCl instead of the corresponding K^+ salts and was titrated with CsOH. Standard extracellular (pipette) solution was as follows: 150 mM NaCl, 2 mM KCl, 1.5 mM $CaCl_2$, 1 mM $MgCl_2$, and 10 mM HEPES, pH 7.38. The osmolarity of the solution was 290 mOsm, and pH was titrated to 7.36–7.38 with NaOH. MTSET solution was made fresh in intracellular (bath) solutions from 100 mM stocks in water, which were stored at −80°C. MTSET stock was freshly diluted into the bath solution and loaded immediately in the perfusion apparatus before the start of MTSET application. Fresh MTSET solution was loaded into the perfusion apparatus every 8 min.

Characterization of the Perfusion Kinetics
A Warner Instruments SF-77A Perfusion Fast-Step system with three-barrel square glass (700 μM internal diameter) was used for rapid solution exchange. Inside-out patches were perfused with standard intracellular solutions at a rate of 0.5 ml/min. Fig. 2 A illustrates the calibration of the solution exchange. The patch was positioned in the center barrel and exposed to the bath solution (140 mM K^+, unfilled portion of bar) at the holding potential. The patch was depolarized from −120 mV to +50 mV for 600 ms, and the barrel was simultaneously switched to a low K^+ solution (50 mM K^+, hatched portion of bar). The duration of the low K^+ exposure was 300 ms. The solution exchange is determined by two factors: a delay (d), followed by a rapid exponential decay characterized by the exchange time constant (τ_e). The time required for complete solution exchange was calculated as d + $4\tau_e$. Fig. 2 B shows the distribution of d and τ_e in a box plot. The medians of d and τ_e were 33 and 4.13 ms, respectively. Characteristics of solution exchange were determined for each patch, and values were used to calculate the correct cumulative modification time for MTSET.
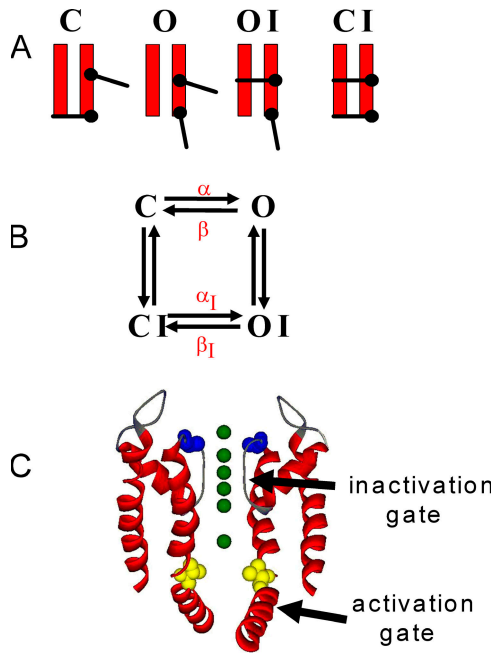
Figure 1. States of the channel. (A) Composite states are depicted with an activation gate (lower gate) and an inactivation gate (upper gate), each in one of two possible configurations. The composite states are C (closed), O (open), OI (inactivated), and CI (inactivated). (B) A simplified four-state gating model with rate constants for the opening (α, α_I) and closing rates (β, β_I) of the activation gate. (C) Structure of the pore region (residues 322–450) made in DS ViewerPro (www.accelrs.com) from Long et al. (2005). Two subunits are shown as ribbon representations, and residues homologous to *Shaker* 449 (blue) and 474 (yellow) are depicted as space-filling atoms. K$^+$ ions are shown as green spheres.

MTSET Modification Measurements

Patches were depolarized from a holding potential of -120 mV to $+50$ mV for the time required to achieve the desired fraction of inactivation. Pulse protocols were run three to four times in the absence of MTSET to verify the stability of the peak currents. Patches showing >5% variability/rundown in peak current were discarded. MTSET (typically 200 μM) was applied for a given time (indicated for each experiment) at either a subsequent hyperpolarized voltage or during a specified depolarization, depending on the state of the channel being probed (Fig. 1 A). These protocols were repeated 7–15 times to determine a time course for modification of V474C (i.e., normalized peak current as a function of cumulative modification time), from which a modification rate constant could be extracted.

Analysis of Data

The cumulative modification time for the nth pulse is

$$(n-1)(L-(d+4\tau_e)), \qquad (1)$$

where L is the duration of the MTSET pulse, and d and τ_e are defined in Fig. 2. A single exponential function was fit to the data points, and the modification rate (ρ) was determined. In the simplest case, this rate is proportional to three terms, as follows:

$$\rho = P_X k_{mod}[\text{MTSET}], \qquad (2)$$

where P_X denotes the probability of being in the MTSET-modifiable state, k_{mod} is the second order rate constant, and [MTSET] is

the MTSET concentration. In all cases, k_{mod} was determined while the inactivation gate was in a steady-state conformation. If the activation gate was either opening or closing during this time (see e.g., Fig. 4 A), a correction for the change in P_O or P_{OI} (P_X in Eq. 2) had to be made. Therefore, P_X was substituted by

$$\int_0^L P_X(t)dt \times P_{X,\max}^{-1} \times L^{-1}, \qquad (3)$$

where $P_{X,\max}$ is the maximal occupancy of state X during MTSET application, and X represents either state O or OI. These corrections were made for modification rates calculated during C→O, OI→CI, and CI→OI transitions. For C→O and CI→OI transitions, the value of Eq. 3 was calculated using $P_X(t) = (1-e^{-t/\tau})^4$ and $P_{X,\max} = 1$, where τ is derived from the current traces elicited at $+50$ mV. For OI→CI transitions, the value of Eq. 3 was calculated using an exponential decay function for $P_{OI}(t)$ based on determination of β_I (see Fig. 5).

Recovery Measurements

To measure recovery, a standard two-step voltage protocol was used. Unless otherwise stated, voltage steps were to $+50$ mV. The first step, used to inactivate channels and measure initial peak current amplitude, was at least fivefold longer than the channel's time constant for inactivation. After a recovery period defined as the interpulse interval (ipi) at -120 mV, the second voltage step was applied and peak recovered current amplitude was measured. No leak subtraction was used. Fractional recovery (FR) was calculated as $(I_2 - I_{ss1})/(I_1 - I_{ss1})$, where I_1 and I_2 represent the peak current amplitudes during the first and second depolarizing step, respectively, whereas I_{ss1} represents the steady-state current at the end of the first depolarization. To determine the time course of recovery from inactivation (see Fig. 3 E), ipi was varied between 0 and 60 s. For the liberation experiments (see Figs. 6 and 7), the ipi was set to give 90% recovery (ipi $\sim$ 21 s; FR $\sim$ 0.9) when K$^+$ was present continuously (see Fig. 6, protocol 1). This procedure for determining ipi was made for every cell before Cs$^+$ trapping and liberation to avoid complicating effects of K$^+$ accumulation on recovery kinetics (Levy and Deutsch, 1996). To ensure complete restoration of current between recovery measurements and maintain viable patches, patches were maintained at -100 mV in K^+_i for $\geq$2 min after the final depolarization in intracellular K$^+$ for a given recovery protocol. Statistical significance of differences in mean FR was determined using a one-way ANOVA on all the data, followed by an all-pairwise multiple comparison (Student-Newman-Keuls method).

RESULTS

To investigate the coupling between activation and inactivation gating, we used two methods: cysteine accessibility and a Cs$^+$ liberation strategy. For these experiments we used a double mutation in the *Shaker*-IR background, as shown graphically in Fig. 1 C (T449A, blue; V474C, yellow). Residue 449 is located in the outer mouth of the pore, and an alanine in this position speeds entry into the slow-inactivated state. The time constant for inactivation of the T449A mutant is $\sim$130 ms at $+50$ mV (Fig. 3 A). Residue 474 faces into the water-filled cavity between the inactivation and activation gates, and accessibility of 474C to hydrophilic modifying reagents reliably tracks the status of the activation gate (Liu et al., 1997). This double mutant was studied in inside-out
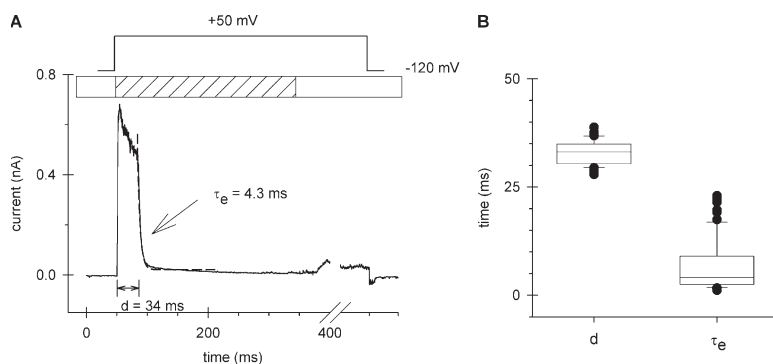
Figure 2. Characterization of the perfusion kinetics. (A) Components of solution exchange. The patch was held at -120 mV in the presence of 150 mM intracellular K$^+$ and depolarized to $+50$ mV for 600 ms with concomitant switching of the intracellular solution to one containing 50 mM K$^+$ for the first 300 ms of the depolarizing step (hatched portion of bar). The kinetics of the solution change are depicted in the current trace as a rapid decrease in current. The mechanical and electrical delay is d, and the fit of a single exponential to the falling phase of the current gives the time constant of the solution exchange, τ_e. (B) Box plots of d and τ_e indicate median values of 33 ms and 4.1 ms, respectively.

patches from *tsA201* cells and exposed to intracellular MTSET to obtain modification rate constants in the open state, at depolarized voltages, and when the channel is inactivated, at both depolarized and hyperpolarized voltages.

Our initial task was to determine the biophysical properties of this T449A/V474C mutant, specifically the voltage dependence of open probability, steady-state inactivation, deactivation, and recovery from slow inactivation (Fig. 3, A–E). These properties dictate the conditions for our experiments and provide a database for comparison of the kinetics of C↔O transitions in the noninactivated and inactivated channel. A Na-based extracellular solution was used in the pipette and a KF/KCl solution in the bath (intracellular solution). The patch was held at -120 mV and depolarized to test potentials ranging from -80 to $+70$ mV in 10-mV increments every 45 s (Fig. 3 A). The voltage dependence of the open probability (P_O) was determined from the peak currents, as described in the legend to Fig. 3 B. The midpoint of the P_O vs voltage curve is -50.5 ± 0.8 mV ($n = 3$). This is in reasonable agreement with V474C *Shaker*-IR, which has an activation midpoint of approximately -58 mV (Liu et al., 1997). A step to $+50$ mV thus ensures that all channels open quickly and that the P_O at this voltage is maximal. By -80 mV, the open probability is close to zero. Similar solutions and configuration were used to determine the voltage dependence of steady-state inactivation (Fig. 3 C; see legend for details); the midpoint is -72.9 ± 2.1 mV ($n = 3$). Therefore, at voltages negative to -80 mV, all channels are in a noninactivated conformation at steady state. Thus, holding potentials in the range of -80 to -120 mV ensure a high probability that channels contain a closed activation gate and an open inactivation gate (Fig. 1 A, composite state C).

In addition to these thermodynamic properties, two kinetic parameters were required to set conditions for this study: closing kinetics of the activation gate (O→C; i.e., deactivation) at negative voltages and recovery kinetics from slow inactivation. The former was determined by standard tail current analysis (a step to the

indicated voltage after a brief 7-ms depolarization to $+50$ mV). A fit of the decaying tail current to a single exponential function gave deactivation time constants (τ_d) of 0.59 ± 0.05 ms ($n = 5$) and 1.03 ± 0.07 ms ($n = 15$) at -120 and -105 mV, respectively (Fig. 3 D). These time constants are comparable to those obtained from *Shaker*-IR (Zagotta et al., 1994). At voltages more hyperpolarized than -80 mV, a channel with a closed activation gate will not reopen. Therefore, in this voltage range the rate of deactivation represents the rate of closure of the activation gate. Recovery at -120 mV, after complete slow inactivation at $+50$ mV (for 1.5 s), was measured using a standard two-pulse protocol (Levy and Deutsch, 1996) to give a recovery time constant (τ_{rec}) of 10.6 ± 0.5 s ($n = 4$; Fig. 3 E). These electrophysiological parameters were used to devise protocols to determine (a) when the activation gate closes after repolarization of the inactivated channel, (b) whether the closed inactivation gate stabilizes the activation gate in a particular configuration, and (c) whether inactivation alters the closing and opening rates of the activation gate. The results of these determinations will reflect whether movement of the activation gate is coupled to the state of the inactivation gate.

Time of Activation Gate Closure in the Inactivated Channel

To assess the open/closed status of the activation gate, we measured the kinetics of modification of V474C, which is only accessible to intracellular cysteine reagents when the activation gate is open (Liu et al., 1997). MTSET modification of V474C renders the channel nonconducting. Inside-out patches were exposed to MTSET during or after appropriate protocols designed to capture channels predominantly in one composite state only, either O, C, OI, or CI. In all cases, the kinetics of solution changes were determined for each patch (see Materials and methods), and this exchange time was used to calculate the correct cumulative modification time for MTSET. In general, solution changes were 90% complete within 20 ms (Fig. 2 and Materials and methods). The rate constant for modification of the open channel was determined by repeated brief depolarizations to
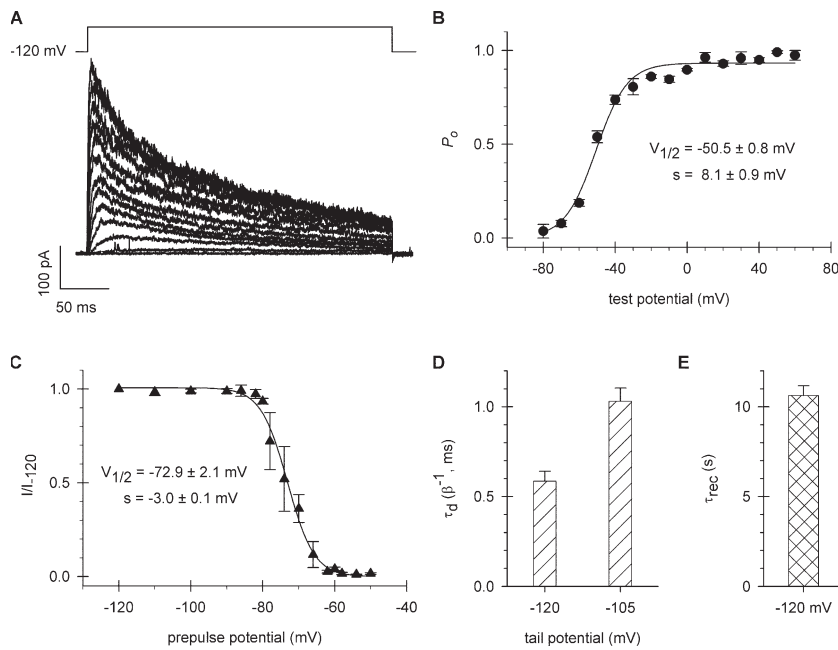
A

-120 mV

100 pA

50 ms

B

P_O

1.0

0.5

0.0

-80   -40   0   40   80

test potential (mV)

$V_{1/2}$ = -50.5 ± 0.8 mV

s = 8.1 ± 0.9 mV

C

I/I_{-120}

1.0

0.5

0.0

-120   -100   -80   -60   -40

prepulse potential (mV)

$V_{1/2}$ = -72.9 ± 2.1 mV

s = -3.0 ± 0.1 mV

D

$\tau_d (\beta^{-1}, ms)$

1.0

0.5

0.0

-120   -105

tail potential (mV)

E

$\tau_{rec} (s)$

10

5

0

-120 mV

Figure 3. Biophysical properties of the channel. (A) Macroscopic K^+ currents in the inside-out configuration. For the composition of the solutions, see Materials and methods. The patch was held at -120 mV and depolarized to test potentials ranging from -80 to $+70$ mV in 10-mV increments every 45 s. The duration of the depolarizing pulses was 300 ms. Sampling frequency was 10 kHz. Data were filtered at 5 kHz. Leak was subtracted online using a P/5 protocol. (B) Voltage dependence of P_O. The P_O at each test potential (●) was calculated as $P_O = I_V/I_{V,t}$, where I_V and $I_{V,t}$ are the peak current and the peak tail current, respectively, measured at membrane potential V. The tail current protocol consisted of a 7-ms step to $+50$ mV, followed by a 10-ms step to a membrane potential ranging from $+70$ to -140 mV. $I_{V,t}$ was measured during the second step. The line shows the best fit Boltzmann function. The mean values ± SEM of the midpoint ($V_{1/2}$) and slope factor (s) are shown ($n = 3$). (C) Voltage dependence of steady-state inactivation. The fraction of noninactivated channels at each voltage (▲) was calculated as I/I_{-120}, where I is the peak current evoked by 7-ms depolarization to $+50$ mV from a prepulse potential applied for 60 s, whereas I_{-120} is the peak current evoked by identical depolarization from the holding potential of -120 mV. The line shows the best fit Boltzmann function. The mean values ± SEM of the $V_{1/2}$ and slope factor are shown ($n = 3$). (D) Deactivation kinetics of the current. In the protocol used, tail currents were evoked by stepping to the indicated membrane potentials after a 7-ms depolarization to $+50$ mV. The deactivation time constant (τ_d) was determined by fitting a single exponential function to the decaying tail currents. The bars indicate the mean + SEM ($n > 5$). The time constant is the reciprocal of the rate constant for channel closure (β) in Fig. 1. (E) Kinetics of recovery from inactivation. In the protocol used, pairs of depolarizing pulses were delivered from the holding potential of -120 to $+50$ mV for 1.5 s. The ipi at -120 mV varied between 0 and 60 s. The FR was calculated as I_2-I_{ss1}/I_1-I_{ss1}, where I_2 and I_1 are the peak currents during the second and first pulse, respectively, and I_{ss1} is the current at the end of the first depolarization. The FR versus ipi plot was fit with an exponential function to give a time constant. Data are given as mean ± SEM ($n = 4$).

$+50$ mV (Fig. 4 A) in the continuous presence of 200 μM of MTSET. The 7-ms duration of the depolarizing pulse is sufficient to completely activate channels but is too short to induce inactivation (Fig. 4 A). A decrease of the peak currents occurs upon repetitive pulsing in the presence of MTSET (Fig. 4 A). The peak currents for each pulse were determined and normalized to the peak current of the first pulse and plotted as a function of cumulative modification time (Fig. 4 B). The modification rate is a product of the probability of being in the MTSET-modifiable state, k_{mod} (the second order modification rate constant for that state), and the MTSET concentration (see Eq. 2 in Materials and methods). The probability of being in the MTSET-modifiable state changes with time, as manifested in the gradual activation of the current (Fig. 4 A). Thus, the integral of this probability must be used to calculate the modification rate constant (see Eq. 3 in Materials and methods). A single exponential function was fit to the data to give a k_{mod} for the open state of $1.28 \times 10^5 \, M^{-1}s^{-1}$. The average of four replicate experiments is $1.31 \times 10^5 \pm 0.19 \times 10^5$ $M^{-1}s^{-1}$ ($n = 4$). These values are consistent with those obtained for V474C in the *Shaker*-IR open channel (Liu et al., 1997).

To evaluate the status of the activation gate in the inactivated channel, two different voltage conditions were used. First, we administered MTSET to the patch at negative voltages. We depolarized a patch to $+50$ mV for 1.5 s to completely inactivate the channels and then repolarized to -120 mV for 400 ms. The 400-ms period is short compared with the time required for recovery ($\tau_{rec} \sim 10$ s at -120 mV; Fig. 3 E); i.e., the channels are still inactivated, but not yet recovered. Then MTSET was applied for 500 ms. This yielded no substantial modification; i.e., there was no decrement in peak current (Fig. 4, C and D). These results suggest that the activation gate closes within 400 ms upon return of the voltage to -120 mV. We suggest that this is the CI state of the channel, which cannot be modified because access of MTSET to 474C is prevented by closure of the activation gate.

Our second evaluation of inactivated channels was designed to study the OI state and was therefore performed at a depolarized voltage. We determined k_{mod} at $+50$ mV, after 800 ms of depolarization at $+50$ mV, which inactivated the channels completely (residual steady-state current was $2.2 \pm 0.2\%$ of the peak current; $n = 45$). Fig. 4 E shows that exposure to MTSET during
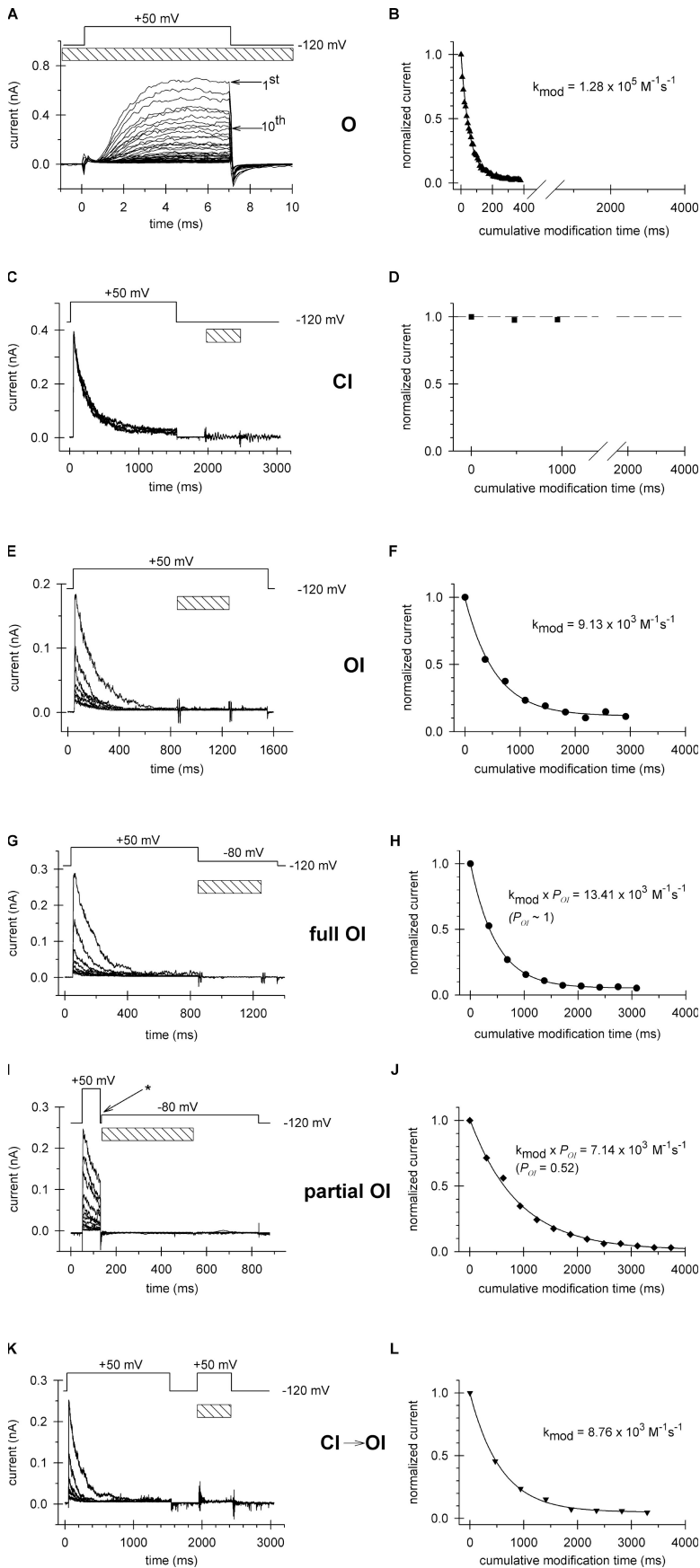
Figure 4. Status of the activation gate. (A, C, E, G, I, and K) Patches were repeatedly depolarized from a holding potential of -120 mV using the pulse protocols shown above the corresponding raw current traces. Pulse protocols, with appropriate interpulse intervals, were run three to four times in the absence of MTSET to verify the stability of the peak currents (not depicted). The timing and the duration (L) of the MTSET pulse are indicated by the hatched bars. A gradual decrease of the peak currents during repetitive pulsing occurred if the activation gate of the channel was open during MTSET application. (B, D, F, H, J, and L) The peak currents for each pulse were determined and normalized to the peak current of the first pulse and plotted as a function of the cumulative modification time, which is calculated using Eq. 1 in Analysis of Data. Values for k_{mod}, shown in B, H, J, and L, are measured modification rates corrected for time-dependent changes in P_O or P_{OI}. (A and B) Depolarizing pulses were applied in the continuous presence of 200 μM MTSET; thus, d and τ_e are both 0 in Eq. 1. The modification rate was corrected by multiplying by 1.39, a factor derived from Eq. 3 using the activation kinetics of the normalized current, $P_O(t) = (1-e^{-t/\tau})^4$ and $P_{O,max} = 1$ (see Analysis of Data). (C and D) [MTSET] = 200 μM, L = 500 ms. MTSET application was initiated 400 ms after returning to -120 mV. (E and F) [MTSET] = 200 μM, L = 400 ms. MTSET application was initiated 800 ms after the start of the depolarization. (G and H) [MTSET] = 200 μM, L = 400 ms. MTSET application was initiated 800 ms after the start of the depolarization. The modification rate was corrected by multiplying by 1.28, a factor derived from Eq. 3 using an exponential decay function for $P_{OI}(t)$ based on determination of β_I (Fig. 5). (I and J) The duration of the depolarizing pulse to $+50$ mV was trimmed to 80 ms to result in $P_{OI} = 0.52$. Note the 5-ms step to -120 mV (indicated by the asterisk), which closed the activation gate of the open channels at the end of the depolarizing pulse (Fig. 1 and Fig. 3). [MTSET] = 200 μM, L = 400 ms. MTSET application was initiated 80 ms after the start of the depolarization. The modification rate was corrected by multiplying by 1.28, a factor derived from Eq. 3 using an exponential decay function for $P_{OI}(t)$ based on determination of β_I (Fig. 5). (K and L) [MTSET] = 200 μM, L = 500 ms. MTSET application was coincident with the second depolarization to $+50$ mV. The modification rate was corrected by multiplying by 1.004, a factor derived from Eq. 3 using a fourth-power function shown above in A and B for $P_O(t)$.

successive depolarizing pulses to +50 mV decreases peak outward current. Normalized current plotted as a function of cumulative modification time was well fit by a single exponential to give a k_{mod} of 9.13×10^3 $M^{-1}s^{-1}$ (Fig. 4 F), only 7% of the rate for the open state. The average k_{mod} was $9.31 \times 10^3 \pm 0.99 \times 10^3$ $M^{-1}s^{-1}$ ($n = 5$). This reduced rate of modification could reflect reduced accessibility/reactivity of V474C in the inactivated channel, or it could represent a small contamination of the channel pool with open channels. This latter possibility was eliminated by the following experiment and analysis. We determined the modification rate for two distinctly different probabilities of the channel being inactivated (P_{OI}). An 800-ms depolarization to +50 mV is sufficient to inactivate 98% of channels (τ_{inact} is 130.4 $\pm$ 7.8 ms at +50 mV; $n = 45$; Fig. 4 G) before repolarization. Thus, an 800-ms depolarization produces a P_{OI} of ~1 (Fig. 4, G and H), whereas an 80-ms depolarization produces a P_{OI} of 0.52 (Fig. 4, I and J). For both cases, we exposed patches to MTSET coincident with repolarization to −80 mV; however, in the latter case ($P_{OI} = 0.52$) a brief (5 ms) repolarization to −120 mV was used before MTSET application to close all open but noninactivated channels. This protocol prevents contamination of the results with modification of the open, noninactivated channels. Patches were exposed to MTSET for 400 ms at –80 mV, a voltage at which k_{mod} is maximal and closed channels do not open (Fig. 3 B). The rates of modification are 13.41×10^3 (Fig. 4 H) and 7.14×10^3 $M^{-1}s^{-1}$ (Fig. 4 J), respectively, a ratio of 0.53. These results demonstrate that the modification rates are proportional to P_{OI} and that a contaminating contribution from open, noninactivated channels does not occur. The reduced modification rate for the inactivated channel reflects reduced accessibility/reactivity of V474C. These results also suggest that the measured modification rate in Fig. 4 (E and F) reflects modification of the inactivated channel alone (i.e., the OI state). This OI state was entered from the open, noninactivated state of the channel at +50 mV. The modification rate for the OI state at −80 mV (Fig. 4 H) is larger than that obtained at +50 mV (Fig. 4 F). Because both the voltage dependence of [MTSET] in the pore and of activation gate opening would each predict a smaller modification rate at −80 mV, the observed increase likely reflects voltage-dependent conformations of the inactivated channel. No such additional voltage dependence exists for noninactivated channels (Liu et al., 1997).

To confirm that we are measuring modification rates of the OI state, we investigated reopening of the channel from the CI state. A transition from CI to OI should produce, at steady state, the same modification rate at +50 mV as channels that have entered the inactivated state directly from the open state. Provided that the final P_{OI} is the same in both cases and that the opening kinetics are comparable, regardless of the pathway, k_{mod} should be the same. To test this hypothesis, we used the reopening protocol shown in Fig. 4 K. After a repolarization period of 400 ms at −120 mV (all channel activation gates have closed; Fig. 3 D), a step to +50 mV for 500 ms, with concomitant MTSET exposure, produces a k_{mod} of 8.76×10^3 $M^{-1}s^{-1}$. The average k_{mod} was $8.59 \times 10^3 \pm 0.88 \times 10^3$ $M^{-1}s^{-1}$ ($n = 4$), in close agreement with that obtained after a direct O→OI transition during the initial depolarization to +50 mV (P > 0.59; Fig. 4 F). In contrast, when channels were first accumulated in the CI state, at −120 mV, and then triggered with a step to −80 mV to equilibrate between CI and OI states, the modification rate was zero; i.e., the activation gate does not open.

Closing Kinetics of the Activation Gate Are Coupled to the State of the Inactivation Gate

In noninactivated channels, the activation gate closes rapidly, with a time constant of ≤1 ms at –120 mV (Fig. 3 D). However, we do not know the kinetics for closure of this gate in inactivated channels. The rate of activation gate closure in inactivated channels was measured using the following strategy. As depicted in Fig. 5 (A and D), complete inactivation of the channels was achieved by a depolarizing pulse to +50 for 800 ms, followed by pulses of varying duration at −120 or −105 mV before MTSET application. During this time at a hyperpolarized voltage, the activation gate may close. Closure of the activation gate within the duration of the hyperpolarizing pulse prevents modification during subsequent exposure to MTSET that is coincident with a step to −80 mV, a voltage at which CI channels do not open. Thus, a channel whose activation gate has closed at −120 or −105 mV in the allotted time of the pulse will remain closed at −80 mV. In contrast, a channel whose activation gate did not close within the allotted time will be modified by MTSET at −80 mV. Thus, the overall modification rate will be proportional to the fraction of channels remaining in the OI state after the hyperpolarizing pulse. That is, as activation gates close, P_{OI} will decrease and therefore, so will the overall modification rate. For example, a 20-ms hyperpolarizing pulse to −120 mV before MTSET application gives an overall rate constant of 5.1×10^3 $M^{-1}s^{-1}$ (Fig. 5 B) and an average of $5.56 \times 10^3 \pm 0.78 \times 10^3$ $M^{-1}s^{-1}$ ($n = 3$), a value that is significantly smaller (P < 0.012) than that obtained in the absence of the hyperpolarizing pulse (Fig. 4 H). This indicates that the activation gate of a substantial fraction of the channels closes within 20 ms at −120 mV. When this determination is made for various pulse durations at −120 mV and plotted as a function of pulse duration, an exponentially decaying curve is obtained (Fig. 5 C). The time constant for this decay, 23 ms, is the reciprocal of the closing rate constant, β_I, for inactivated channels. A similar determination at −105 mV
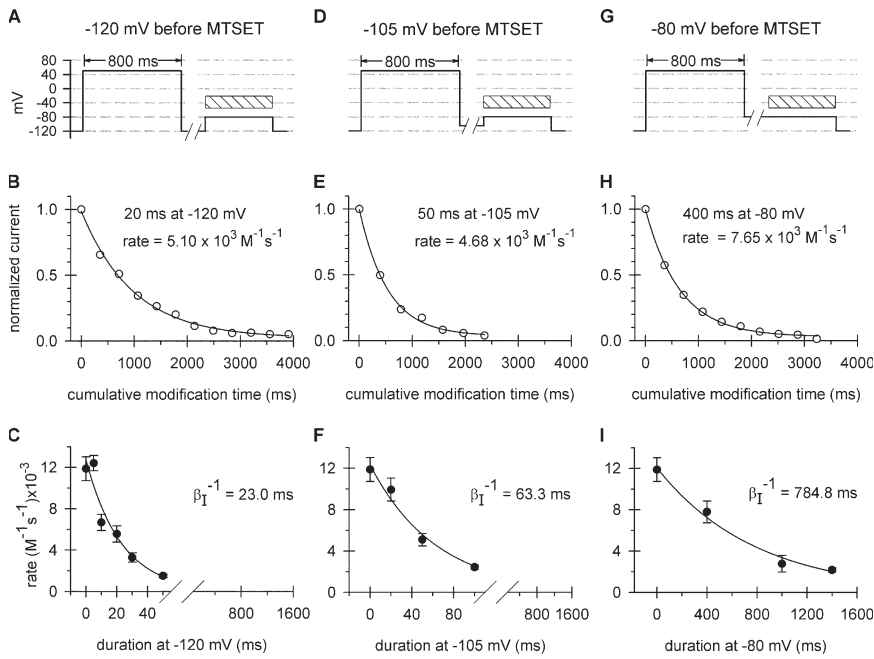
Figure 5. Rate of activation gate closure in the inactivated channel. The pulse protocols (A, D, and G) were based on Fig. 4 I, with the following modification: complete inactivation of the channels was followed by pulses of varying duration at -120 (A–C), -105 (D–F), or -80 (G–I) mV before MTSET application. In all cases, MTSET was applied at -80 mV for 400 ms (hatched bar). This membrane potential is optimal for determining the status of the activation gate (Fig. 3, B and C; and Fig. 4). MTSET concentration was adjusted to achieve complete modification of the channels in <10 episodes (B, 200 µM; E, 400 µM; H, 200 µM). (C, F, and I) Modification rate constants are plotted as a function of pulse duration at -120 (C), -105 (F), or -80 (I) mV preceding MTSET application. The data points were fit with a single exponential function to give the indicated time constants, which are reciprocals of the rate constants (β_I^{-1}) characterizing the OI→CI transition (Fig. 1 B).

(Fig. 5, E and F) yields a time constant of 63.3 ms. Both of these closing time constants are much larger than the corresponding deactivation time constants obtained from the tail currents for noninactivated channels (Fig. 3 D). To determine the closing rate for the activation gate at -80 mV, patches were returned to -80 mV after complete inactivation at $+50$ mV and exposed to MTSET after variable periods of time at -80 mV. For example, channels modified at -80 mV for 400 ms with a 400-ms delay after the end of the voltage step to $+50$ mV show an average rate constant of $7.79 \times 10^3 \pm 1.04 \times 10^3 \, \mathrm{M^{-1}s^{-1}}$ ($n = 3$; Fig. 5 H). The dependence of k_{mod} at -80 mV on duration at -80 mV before MTSET modification reveals a closing time constant of 785 ms, which is, again, substantially slower (100-fold) than deactivation of noninactivated channel. Two conclusions are apparent. First, as with noninactivated channels, the deactivation kinetics are voltage dependent, slowing with increasing depolarization. Second, a closed inactivation gate slows closing of the activation gate.

Opening Kinetics of the Activation Gate Are Coupled to the State of the Inactivation Gate

To determine the influence of the inactivation gate on the closed-open equilibrium of the activation gate, we must either directly assess the open probability of the inactivated state (P_{OI}) or assess both the opening and closing rates of the activation gate (as defined in Fig. 1 B) and compare these parameters with those for the non-inactivated state. In a two-state model, C↔O or CI↔OI, the steady-state value of P_O or P_{OI} will be the ratio $\alpha/(\alpha + \beta)$ or $\alpha_I/(\alpha_I + \beta_I)$, respectively. These determinations are simplistic for both inactivated and noninactivated channels, in part because a two-state gating

model is invalid for most Kv channels. Moreover, because P_{OI} is a function of both opening and closing rates, a determination of β_I alone (Fig. 5) is insufficient to determine P_{OI}. Opening kinetics must also be considered. The challenge here is to measure the opening of the activation gate of inactivated channels that do not produce measurable currents. To overcome this obstacle, we chose a strategy previously introduced to measure liberation of a trapped cation in inactivated *Shaker*-IR channels as an indicator of the opening of the activation gate (Ray and Deutsch, 2006). This method uses a multistep protocol and relies on trapping an intracellular cesium ion (Cs^+) in the inactivated channel upon repolarization after a long depolarization. A trapped Cs^+ ion in the inactivated channel causes the channel to recover slowly (measured by a third depolarizing pulse). If the trapped Cs^+ is liberated before recovery, e.g., by opening the activation gate in the presence of intracellular K^+ (second pulse), then the channel will recover at a rate commensurate with the recovery rate when a K^+ ion is trapped in the channel (Ray and Deutsch, 2006). That is, the liberated Cs^+ ion is replaced by a K^+ ion. Thus, recovery kinetics can reveal whether a depolarization is long enough in duration for the activation gate to open and liberate a Cs^+ ion.

Protocol 4 (Fig. 6) shows the liberation protocol, including the initial depolarizing pulse (a step to $+50$ mV for 800 ms), followed in the presence of intracellular Cs^+ by a step to -120 mV, which traps the Cs^+ in the channel. We then applied the liberation pulse, a step to the indicated voltage for various durations, which liberates Cs^+, replacing it with K^+. A subsequent depolarization to $+50$ mV (the final pulse, ~21 s later; see Materials and methods) is used to measure the FR. At -120 mV,
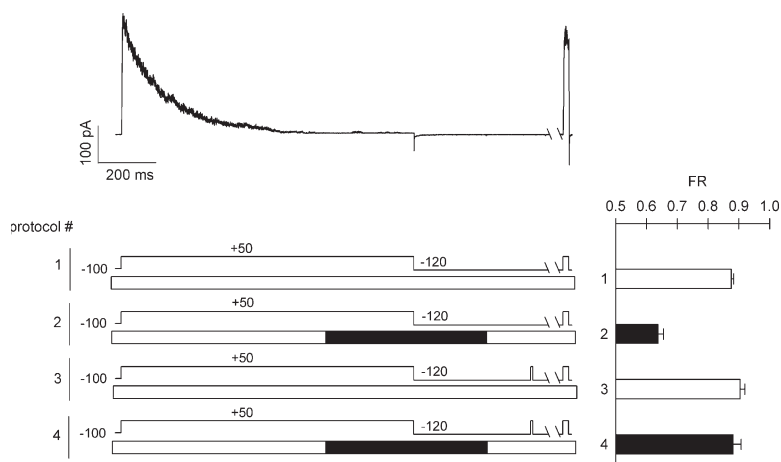
Figure 6. Cs+i trapping and liberation. After inactivation, FR was measured using an ipi that gave 90% recovery when K$^+$ was present continuously (raw current trace, ipi = 21 s), which corresponds to protocol 1. The open bar indicates perfusion of the patch with KF/KCl intracellular solution. Protocol 2 indicates that a Cs$^+$i pulse (shaded portion of the bar) was applied so as to overlap with the transition from depolarized (+50mV) to hyperpolarized (−120 mV) membrane potential (total pulse duration was 550 ms, including 300 ms at +50 mV and 250 ms at −120 mV). Cs$^+$i was washed out by reperfusion with the KF/KCl solution. Protocol 3 indicates that K$^+$ was present continuously but that a 7-ms depolarizing voltage step was applied to reopen the activation gate. This latter pulse was applied 400 ms after initially returning to −120 mV. In protocol 4, a Cs+i pulse was applied (identical to that in protocol 2), and Cs$^+$i was washed out, followed by a 7-ms depolarizing voltage step to +50 mV to reopen the channel. This latter pulse was applied 400 ms after initially returning to −120 mV and results in exchange of Cs$^+$ for K$^+$. Protocol 4 tests the ability of a depolarizing pulse to +50 mV to restore FR to levels observed after repolarization in K$^+$ only. Bars at right show resulting FR (n ≥ 3). Cs$^+$-exposed channels deprived of a liberation pulse yield lower FRs than non–Cs$^+$-exposed chan-nels (P < 0.05).

in the presence of K^+_i only, the FR is 0.88 ± 0.01 ($n = 16$; Fig. 6, protocol 1). In Cs^+_i, FR is 0.64 ± 0.02 ($n = 17$; protocol 2). Whether K^+_i is present continuously or a trapped Cs$^+$ is liberated by a voltage step to +50 mV for 7 ms, recovery is virtually identical: FR is 0.90 ± 0.02 ($n = 3$; protocol 3) and 0.88 ± 0.03 ($n = 4$; protocol 4), respectively. At +50 mV the Cs$^+$ is completely liberated within 7 ms (Fig. 6 and Fig. 7 A).

Fig. 7 A shows that the time course of liberation of Cs$^+$ from the inactivated channel (i.e., increase in FR with increasing duration of the liberating pulse; red circles) superimposes on the activation kinetics of the current elicited at +50 mV from a noninactivated channel. This comparison is meaningful and bears on the relative kinetics of activation and movement of the activation gate in the inactivated and noninactivated channels as follows. At a voltage as depolarized as +50 mV, the closing rate of the activation gate is presumably negligible, regardless of whether the channel is in state O or OI. If the closing rate is very small, the kinetics of activation gate opening (either $P_O(t)$ or $P_{OI}(t)$) is the same as the kinetics of first reaching the open state (Horn, 1984). Moreover, these first-latency kinetics describe the time course of liberation, assuming that the Cs$^+$-K$^+$ exchange is rapid when the activation gate is open (see Discussion in Ray and Deutsch, 2006). Therefore, the superposition in Fig. 7 A indicates that at +50 mV inactivation has no effect on opening kinetics of the activation gate. At more hyperpolarized voltages, however, where the closing rate (β or β$_I$) is not negligible, the kinetics of activation gate opening (i.e., $P_O(t)$ or $P_{OI}(t)$) will in general be faster than the first-latency opening kinetics of the activation gate after a depolarization (see legend to Fig. 7). The first-latency kinetics is not a function of closing rates, whereas the

activation kinetics includes eigenvalues that are functions of the sum of rates both entering and leaving the open state and is thus faster. To intuit this, consider the simple two-state model depicted in Fig. 1. The first latency rate (eigenvalue) is α and the activation rate is α + β, which is greater than α alone. Therefore, at sufficiently hyperpolarized voltages, where $P_O(\infty)$ is <1, a comparison of activation and liberation kinetics has further significance. Specifically, if the rate of liberation is faster than or equal to that of activation, then the CI→OI transition (opening rate in the inactivated channel) must be faster than the C→O transition (opening rate in the noninactivated channel).

At −50 mV, where P_O is ∼0.5 at steady state for non-inactivated channels (Fig. 3 B), Cs$^+$ liberation kinetics were indistinguishable from those of channel activation (Fig. 7 B), as at +50 mV (Fig. 7 A). This result shows that the rate of activation gate opening in inactivated channels is greater than in noninactivated channels at −50 mV. We extended these measurements to more hyperpolarized voltages. Initially, we assessed FR using long durations (e.g., 300 ms) for the liberation pulses of −55, −60, and −70 mV (Fig. 7 D). The FR decreased monotonically from −55 to −70 mV; in the latter case, no channels reopened within 300 ms to liberate the trapped Cs$^+$. At −60 mV, the liberation kinetics were too slow to measure accurately (unpublished data). The activation kinetics at −60 mV of noninactivated channels, however, displayed a time constant of ∼14 ms, clearly faster than the liberation kinetics. A comparison of the two sets of kinetics was nevertheless possible using a slightly less negative voltage. At −55 mV, liberation kinetics of inactivated channels were clearly slower than activation kinetics of noninactivated channels (Fig. 7 C). Moreover, both activation kinetics and liberation
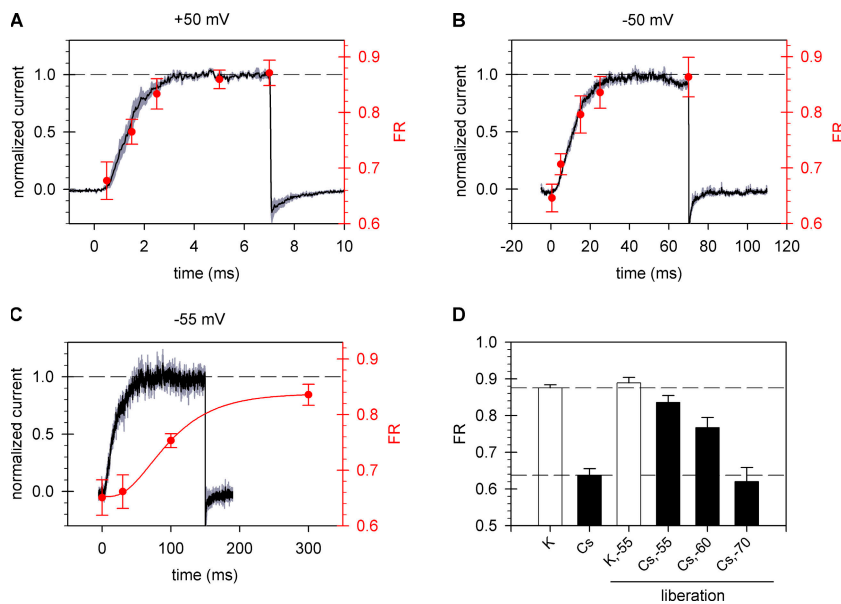
Figure 7. Rate of activation gate opening in inactivated channels. (A–C) Kinetics of activation and liberation after Cs^+ loading and unloading of the inactivated channel. Liberation was performed at +50 (A), −50 (B), or −55 (C) mV. The black trace shows normalized current (left y axis) after a step to the indicated voltage ($n = 3$). Gray swaths on either side of the line represent standard error of the current amplitude. Red circles show FR (right y axis) measured using a protocol similar to that shown in Fig. 6 (protocol 4), except that the liberation step was to the indicated voltage and the step duration was varied as indicated, depending on the liberation voltage. Data are represented as means ± SEM ($n \geq 3$). In C, the continuous red line represents a fit of the data to a fourth-power sigmoidal function. Activation time constants measured from current traces are 0.94 ± 0.02 ($n = 4$), 5.9 ± 0.28 ($n = 14$), and 9.4 ± 1.05 ms ($n = 6$) for +50, −50, and −55 mV, respectively. (D) FR after steady-state liberation. FR was measured according to protocol 4 (Fig. 6) after a liberation pulse of 300 ms at −55, −60, and −70 mV (shaded bars labeled as Cs,−55; Cs,−60; and Cs,−70, respectively). For comparison, FR was also measured for channels held continuously at −120 mV and exposed to K^+_i only (open bar labeled as K) or to Cs^+_i only (shaded bar labeled as Cs), or to K^+_i only, but subject to a depolarization to −55 mV (open bar labeled as K,−55) for 300 ms (protocols 1, 2, and 3, respectively, in Fig. 6). Because the 300-ms depolarization to −55 mV in K^+_i did not affect FR, no additional controls were necessary for −60 and −70 mV. FRs for −55, −60 and −70 mV are significantly different based on a two-step statistical analysis. First, a one-way ANOVA was performed on all the data, followed by an all-pairwise multiple comparison (Student-Newman-Keuls method) to give a P value <0.05 in all cases. Extensive simulations using linear multistate gating models with one open state showed that in all cases (i.e., widely varied values of rate constants) the normalized $P_O(t)$ is always greater than or equal to the time-dependent first latency for reaching the open state in the same model. This observation leads to our general conclusion that activation kinetics are never slower than liberation kinetics at the same voltage, unless gating rate constants differ between inactivated and noninactivated channels.

kinetics are slower at −55 mV than at −50 mV, in part reflecting the voltage dependence of activation gate opening. The discrepancy between the kinetics of liberation and activation shown in Fig. 7 C does not, unfortunately, offer a conclusive interpretation about activation gate opening at this voltage. As mentioned earlier, it is only when liberation kinetics are comparable to or faster than activation kinetics that we can make an unambiguous comparison of activation gate opening for inactivated and noninactivated channels. Nevertheless, we have demonstrated that the closing rate of the activation gate is decreased by inactivation (Fig. 5) and that the opening rate at −50 mV is increased by inactivation (Fig. 7 B). The composite results therefore indicate that a closed inactivation gate energetically favors an open activation gate and that inactivation alters both the closing and opening rates of the activation gate.

DISCUSSION

The composite closed (C) and open (O) states of *Shaker*-IR have been well studied and are defined by the position of the gates as depicted in Fig. 1. There is no ambiguity regarding the existence of the closed and open states or their timed occurrence, because they are directly assessed from the presence of ionic currents or lack thereof. Lack of conductance at very negative voltages has been attributed to a channel with a closed activation gate, despite in some cases a tremendous electrochemical driving force on ions to move across the membrane. Conductance at very positive voltages is a sign that the activation gate is open. In contrast, the nature of CI and OI states of the channel, as depicted in Fig. 1 A, is less substantiated. Moreover, the assignment of these states to specific kinetic phases of channel behavior is also ambiguous. For example, there has been no direct temporal characterization of the status of the activation gate in the inactivated channel. The difficulty lies in the fact that the inactivated state is nonconducting and thus current cannot tell us about the open/closed status of the activation gate. It has been suggested that inactivated channels have a higher Na^+ permeability relative to K^+ vis-à-vis the open state (Starkus et al., 1997; Starkus et al., 1998; Kiss et al., 1999; Wang et al., 2000a) and even that multiple inactivated states exist, including one that is only permeable to Na^+ and through which an inactivated channel must move to deactivate and recover (the "R" state; Wang et al., 2000a). These observations led Fedida and co-workers to use Na^+ tail currents as a readout for the inactivated state of Kv1.5 channel (Wang et al., 2000b; Wang and Fedida, 2001; Wang and Fedida, 2002; Kurata et al.,

2004). However, the R state may not represent the inactivated state. It may only exist when K^+ ions normally bound to sites in the selectivity filter are replaced with Na^+ ions, which occurs under unusual ionic conditions that may themselves distort the selectivity filter (Zhou et al., 2001b). Moreover, the kinetics of the Na^+ tails are difficult to interpret unambiguously. They reflect changes in macroscopic conductance and could be caused by changes in single-channel conductance, selectivity, and/or gating at the selectivity filter, and not to changes in activation gating. Despite these attempts to characterize the inactivated states, several questions remained unanswered. For example, precisely when does the activation gate close when an inactivated channel is hyperpolarized? Is movement of the activation gate coupled to inactivation gating?

To more directly and unambiguously address these issues, we chose an accessibility assay, similar to that first used by Yellen and co-workers to locate the activation gate in the lower portion of S6 (Liu et al., 1997; del Camino and Yellen, 2001). The results displayed in Fig. 4 constitute evidence for the existence of CI and OI states, i.e., states in which the activation gate is closed (CI) or open (OI) in the inactivated channel. Within 400 ms of returning completely inactivated channels to a hyperpolarized voltage, no modification of V474C occurs (Fig. 4). This is the CI state. The activation gate has closed, yet the channel is still inactivated and does not completely recover until ~50 s later. Because the time constant for closure of the activation gate is 23 ms in an inactivated channel at -120 mV (Fig. 5), ~500-fold faster than the recovery rate at this voltage, the rate-limiting step for recovery is not closure of the activation gate. The existence of an inactivated channel with an open activation gate (i.e., the OI state) is clearly demonstrated by the rate of MTSET modification at $+50$ mV after a prolonged depolarization and decrease of the outward ionic current to ~2% of the peak amplitude. The activation gate remains open despite the lack of current. This is the OI state. Our results are consistent with those of Kurata et al. (Kurata et al., 2004), who showed that the N-terminal fast inactivation peptide and TEA can access the central cavity when the channel is slow inactivated at positive membrane potentials. Our clear demonstration of a voltage-dependent OI↔CI equilibrium suggests that the pathway for recovery at hyperpolarized voltages is from OI to CI to C.

The lower k_{mod} for the OI state (9.31×10^3 $M^{-1}s^{-1}$) versus the open state (1.31×10^5 $M^{-1}s^{-1}$), both at $+50$ mV, could reflect a different accessibility/environment for V474C in the cavity of an inactivated channel than in the open channel, each state having an open activation gate. Alternatively, the nonzero value of k_{mod} could reflect a small fraction of open channels that are modified because flickering between inactivated (OI) and noninactivated (O) channels, each with open activa-

tion gates, leads to the inactivation gate being open ~2% of the time at steady state. We favor the former hypothesis, because under conditions in which there are no noninactivated channels (i.e., -80 mV), we still observe a k_{mod} that is substantially different from the modification rate for the open (O) state. This argues strongly that the lower modification rate likely reflects an altered conformation of the cavity in the inactivated state compared with the cavity in the open state. Such an altered conformation could be very slight and yet have a profound effect. An altered conformation of the inactivated state is consistent with the block of Kv1.3 by small-molecule inhibitors that bind to the pore at intracellular sites and are specific for the slow-inactivated state (Hanner et al., 2001).

The activation pathway includes several steps and pre-open closed states of the channel, thus complicating a simple analysis of activation gate opening kinetics. Closure of the activation gate, however, may be considered as a single transition from the open state to a preopen closed state. This rate is β (or β_I). Two considerations preclude the use of a simple analysis of the kinetics to determine open probabilities, i.e., $P_{OI} = \alpha_I / (\alpha_I + \beta_I)$. First, as stated in the Results, activation is a multistep process. Second, we cannot precisely determine both the opening and the closing kinetics of the activation gate in the inactivated channel at the same voltage. Nonetheless, we may draw a valid conclusion: closing of the inactivation gate stabilizes the activation gate in the open position. At hyperpolarized voltages the activation kinetics are faster (Cs^+ liberation experiment) and closing kinetics are slower (MTSET experiment) relative to the noninactivated channel; therefore, the P_{OI} must increase relative to P_O at hyperpolarized voltages.

What is the mechanism for stabilization of the open state in the inactivated channel? Thus far, we do not have an atomic level structure of the inactivated state of a voltage-gated K^+ channel. However, several structural studies of KcsA have suggested that the conformation of the inactivated channel includes altered ion occupancy in the selectivity filter of the pore (Lenaeus et al., 2005), rearrangement of residues in the outer mouth/turret (Liu et al., 1996; Cordero-Morales et al., 2006), and gross distortions of the selectivity filter itself (Zhou et al., 2001b). Whether any of these pertain to the *Shaker*-IR inactivated channel and provide clues to the mechanism by which the inactivation gate alters activation kinetics is not yet known. However, functional experiments provide clues. Thermodynamic mutant cycle analyses demonstrate that gating-sensitive residues that are as much as 15Å apart in S6 are coupled to each other (Yifrach and MacKinnon, 2002). These residues cluster mainly in the bundle-crossing region of the activation gate and the upstream region where S6 contacts the pore helix. Yifrach and MacKinnon suggest that pore opening involves simultaneous changes in both

regions and that S6 moves as a rigid body. These features could underlie the crosstalk we observe between activation and inactivation gates. Moreover, because movement of the activation gate is coupled to voltage-sensor movement (Sigworth, 1994; Bezanilla, 2000), our demonstration of coupling between the inactivation and activation gates predicts that inactivation gate closure should slow the return of voltage sensors to their resting states at a hyperpolarized voltage. That is, inactivation should cause charge immobilization in gating current measurements. Studies by Olcese et al. confirm these predictions (Olcese et al., 1997).

Regardless of the mechanism by which these two gates are coupled, the cross talk between them will surely affect cell excitability because inactivation (slow and fast) governs the amount of available K^+ current in a cell. It is this conductance that contributes critically to the resting membrane potential, the shape and frequency of the action potential, and repolarization of the membrane in the final phases of an action potential, all of which influence other membrane potential–dependent processes (e.g., neurotransmitter release; Dodson and Forsythe, 2004). Thus, slow inactivation, including both entry into and exit from the inactivated state, will regulate cell function in at least two ways: one that is direct and one that modulates excitability through its coupled effects on activation gating. Both activation and slow inactivation are commonly found in voltage-gated channels and play very important physiological roles in nonexcitable as well as excitable cells. It is therefore likely that the cross talk we have demonstrated between activation and inactivation gates for *Shaker*-IR is widespread and critical.

REFERENCES

Ashcroft, F.M. 2000. Ion Channels and Disease: Channelopathies. Academic Press, San Diego. 481 pp.

Baukrowitz, T., and G. Yellen. 1995. Modulation of K+ current by frequency and external [K+]: a tale of two inactivation mechanisms. *Neuron*. 15:951–960.

Bezanilla, F. 2000. The voltage sensor in voltage-dependent ion channels. *Physiol. Rev.* 80:555–592.

Choi, K.L., R.W. Aldrich, and G. Yellen. 1991. Tetraethylammonium blockade distinguishes two inactivation mechanisms in voltage-activated K+ channels. *Proc. Natl. Acad. Sci. USA*. 88:5092–5095.

Cordero-Morales, J.F., L.G. Cuello, Y. Zhao, V. Jogini, D.M. Cortes, B. Roux, and E. Perozo. 2006. Molecular determinants of gating at the potassium-channel selectivity filter. *Nat. Struct. Mol. Biol.* 13:311–318.

del Camino, D., and G. Yellen. 2001. Tight steric closure at the intracellular activation gate of a voltage-gated K(+) channel. *Neuron*. 32:649–656.

del Camino, D., M. Holmgren, Y. Liu, and G. Yellen. 2000. Blocker protection in the pore of a voltage-gated K+ channel and its structural implications. *Nature*. 403:321–325.

Demo, S.D., and G. Yellen. 1991. The inactivation gate of the *Shaker* K+ channel behaves like an open-channel blocker. *Neuron*. 7:743–753.

Ding, S., and R. Horn. 2002. Tail End of the S6 Segment: Role in Permeation in *Shaker* Potassium Channels. *J. Gen. Physiol.* 120:87–97.

Dodson, P.D., and I.D. Forsythe. 2004. Presynaptic K+ channels: electrifying regulators of synaptic terminal excitability. *Trends Neurosci*. 27:210–217.

Hanner, M., B. Green, Y.D. Gao, W.A. Schmalhofer, M. Matyskiela, D.J. Durand, J.P. Felix, A.R. Linde, C. Bordallo, G.J. Kaczorowski, et al. 2001. Binding of correolide to the K(v)1.3 potassium channel: characterization of the binding domain by site-directed mutagenesis. *Biochemistry*. 40:11687–11697.

Holmgren, M., M.E. Jurman, and G. Yellen. 1996. N-Type Inactivation and the S4-S5 Region of the *Shaker* K+ Channel. *J. Gen. Physiol.* 108:195–206.

Horn, R. 1984. Gating of channels in nerve and muscle: a stochastic approach. W.D. *Current Topics in Membranes and Transport*. 21:53–97.

Hoshi, T., W.N. Zagotta, and R.W. Aldrich. 1990. Biophysical and molecular mechanisms of *Shaker* potassium channel inactivation. *Science*. 250:533–538.

Hoshi, T., W.N. Zagotta, and R.W. Aldrich. 1991. Two types of inactivation in *Shaker* K+ channels: effects of alterations in the carboxy-terminal region. *Neuron*. 7:547–556.

Jurman, M.E., L.M. Boland, Y. Liu, and G. Yellen. 1994. Visual identification of individual transfected cells for electrophysiology using antibody-coated beads. *Biotechniques*. 17:876–881.

Kiss, L., J. LoTurco, and S.J. Korn. 1999. Contribution of the selectivity filter to inactivation in potassium channels. *Biophys. J.* 76:253–263.

Kozak, M. 1991. Structural features in eukaryotic mRNAs that modulate the initiation of translation. *J. Biol. Chem.* 266:19867–19870.

Kurata, H.T., Z. Wang, and D. Fedida. 2004. NH_2-Terminal Inactivation Peptide Binding to C-Type–Inactivated Kv Channels. *J. Gen. Physiol.* 123:505–520.

Lenaeus, M.J., M. Vamvouka, P.J. Focia, and A. Gross. 2005. Structural basis of TEA blockade in a model potassium channel. *Nat. Struct. Mol. Biol.* 12:454–459.

Levy, D., and C. Deutsch. 1996. Recovery from C-type inactivation is modulated by extracellular potassium. *Biophys. J.* 70:798–805.

Liu, Y., M. Holmgren, M.E. Jurman, and G. Yellen. 1997. Gated access to the pore of a voltage-dependent K+ channel. *Neuron*. 19:175–184.

Liu, Y., M.E. Jurman, and G. Yellen. 1996. Dynamic rearrangement of the outer mouth of a K+ channel during gating. *Neuron*. 16:859–867.

Long, S.B., E.B. Campbell, and R. MacKinnon. 2005. Crystal structure of a mammalian voltage-dependent *Shaker* family K+ channel. *Science*. 309:897–903.

Loots, E., and E.Y. Isacoff. 1998. Protein Rearrangements Underlying Slow Inactivation of the *Shaker* K+ Channel. *J. Gen. Physiol.* 112:377–389.

Margolskee, R.F., P. Kavathas, and P. Berg. 1988. Epstein-Barr virus shuttle vector for stable episomal replication of cDNA expression libraries in human cells. *Mol. Cell. Biol.* 8:2837–2847.

Margolskee, R.F., B. McHendry-Rinde, and R. Horn. 1993. Panning transfected cells for electrophysiological studies. *Biotechniques*. 15:906–911.

Ogielska, E.M., W.N. Zagotta, T. Hoshi, S.H. Heinemann, J. Haab, and R.W. Aldrich. 1995. Cooperative subunit interactions in C-type inactivation of K channels. *Biophys. J.* 69:2449–2457.

Olcese, R., R. Latorre, L. Toro, F. Bezanilla, and E. Stefani. 1997. Correlation between Charge Movement and Ionic Current during Slow Inactivation in *Shaker* K+ Channels. *J. Gen. Physiol.* 110:579–589.

Panyi, G., Z. Sheng, L. Tu, and C. Deutsch. 1995. C-type inactivation occurs by a cooperative mechanism. *Biophys. J.* 69:896–904.

Ray, E., and C. Deutsch. 2006. A Trapped Intracellular Cation Modulates K^+-Channel Recovery from Slow Inactivation. *J. Gen. Physiol.* 128:203–217.

Sigworth, F.J. 1994. Voltage gating of ion channels. *Q. Rev. Biophys.* 27:1–40.

Starkus, J.G., L. Kuschel, M.D. Rayner, and S.H. Heinemann. 1997. Ion Conduction through C-Type Inactivated *Shaker* Channels. *J. Gen. Physiol.* 110:539–550.

Starkus, J.G., L. Kuschel, M.D. Rayner, and S.H. Heinemann. 1998. Macroscopic Na^+ Currents in the "Nonconducting" *Shaker* Potassium Channel Mutant W434F. *J. Gen. Physiol.* 112:85–93.

Wang, Z., and D. Fedida. 2001. Gating charge immobilization caused by the transition between inactivated states in the Kv1.5 channel. *Biophys. J.* 81:2614–2627.

Wang, Z., and D. Fedida. 2002. Uncoupling of Gating Charge Movement and Closure of the Ion Pore during Recovery from Inactivation in the Kv1.5 Channel. *J. Gen. Physiol.* 120:249–260.

Wang, Z., J.C. Hesketh, and D. Fedida. 2000a. A high-Na(+) conduction state during recovery from inactivation in the K(+) channel Kv1.5. *Biophys. J.* 79:2416–2433.

Wang, Z., X. Zhang, and D. Fedida. 2000b. Regulation of transient Na+ conductance by intra- and extracellular K+ in the human delayed rectifier K+ channel Kv1.5. *J. Physiol.* 523(Pt 3): 575–591.

Yellen, G. 1998. The moving parts of voltage-gated ion channels. *Quarterly Review of Biophysics.* 31:239–295.

Yifrach, O., and R. MacKinnon. 2002. Energetics of pore opening in a voltage-gated K(+) channel. *Cell.* 111:231–239.

Zagotta, W.N., T. Hoshi, J. Dittman, and R.W. Aldrich. 1994. *Shaker* Potassium Channel Gating. II: Transitions in the Activation Pathway. *J. Gen. Physiol.* 103:279–319.

Zhou, M., J.H. Morais-Cabral, S. Mann, and R. MacKinnon. 2001a. Potassium channel receptor site for the inactivation gate and quaternary amine inhibitors. *Nature.* 411:657–661.

Zhou, Y., J.H. Morais-Cabral, A. Kaufman, and R. MacKinnon. 2001b. Chemistry of ion coordination and hydration revealed by a K+ channel-Fab complex at 2.0 Å resolution. *Nature.* 414:43–48.